EUROPEAN ORGANIZATION FOR NUCLEAR RESEARCH (CERN)

CERN-PH-EP-2015-123
LHCb-PAPER-2015-011
September 21, 2015

Measurement of the exclusive Υ production cross-section in pp collisions at $\sqrt{s} = 7\,\text{TeV}$ and $8\,\text{TeV}$

The LHCb collaboration[†]

Abstract

A study is presented of central exclusive production of $\Upsilon(nS)$ states, where the $\Upsilon(nS)$ resonances decay to the $\mu^+\mu^-$ final state, using pp collision data recorded by the LHCb experiment. The cross-section is measured in the rapidity range $2 < y(\Upsilon) < 4.5$ where the muons are reconstructed in the pseudorapidity range $2 < \eta(\mu^\pm) < 4.5$. The data sample corresponds to an integrated luminosity of $2.9\,\text{fb}^{-1}$ and was collected at centre-of-mass energies of 7 TeV and 8 TeV. The measured $\Upsilon(1S)$ and $\Upsilon(2S)$ production cross-sections are

$$\begin{aligned}\sigma(pp \to p\Upsilon(1S)p) &= 9.0 \pm 2.1 \pm 1.7 \text{ pb and} \\ \sigma(pp \to p\Upsilon(2S)p) &= 1.3 \pm 0.8 \pm 0.3 \text{ pb},\end{aligned}$$

where the first uncertainties are statistical and the second are systematic. The $\Upsilon(1S)$ cross-section is also measured as a function of rapidity and is found to be in good agreement with Standard Model predictions. An upper limit is set at 3.4 pb at the 95% confidence level for the exclusive $\Upsilon(3S)$ production cross-section, including possible contamination from $\chi_b(3P) \to \Upsilon(3S)\gamma$ decays.

Published in JHEP

[†]Authors are listed at the end of this paper.

1 Introduction

Central exclusive production (CEP) of $\Upsilon(nS)$ ($n = 1, 2, 3$) resonances in pp collisions is thought to occur by photoproduction through the exchange of a photon and a pomeron (a colour-singlet system) between two protons, as illustrated in Fig. 1. Since the protons do not dissociate, typically only a small component of momentum transverse to the beam direction ($p_{\rm T}$) is exchanged in the interaction. The photoproduction of Υ resonances at LHCb can be computed using perturbative quantum chromodynamics (QCD), given the high photon-proton centre-of-mass energy, W, and the cross-section depends on the square of the gluon parton-density function, $g(x)$, where Bjorken-x is the fraction of the proton's momentum carried by the gluon [1]. Measurements of the production cross-sections for the $\Upsilon(nS)$ resonances in the forward region covered by the LHCb detector are sensitive to $g(x)$ in the region of small x down to approximately 1.5×10^{-5}, where the knowledge of $g(x)$ is limited. Furthermore, predictions for the $\Upsilon(nS)$ cross-sections at leading order (LO) and next-to-leading order (NLO) in the strong-interaction coupling differ greatly for the values of W probed in $\Upsilon(nS)$ resonance production, and there are significant variations depending on the models used to describe the Υ wave function and the t-channel exchange [1–3].

Quarkonia photoproduction has been studied in exclusive production at HERA [4–9], the Tevatron [10] and the LHC [11–13]. At LHCb, exclusive production is associated with the absence of significant detector activity apart from that associated with the exclusive candidate. The background from proton dissociation occurring outside the detector acceptance is characterised as having a value of Υ candidate p_T which is larger than that for exclusive production.

In this article, the exclusive production cross-section of $\Upsilon(nS)$ resonances is measured in the $\mu^+\mu^-$ final state where both muons lie in the pseudorapidity (η) range $2 < \eta(\mu^\pm) < 4.5$ and the $\Upsilon(nS)$ candidate is reconstructed in the rapidity (y) range $2 < y(\Upsilon(nS)) < 4.5$. The pp data correspond to an integrated luminosity of $0.9\,{\rm fb}^{-1}$ at a pp centre-of-mass energy of $\sqrt{s} = 7\,{\rm TeV}$ and $2.0\,{\rm fb}^{-1}$ at $\sqrt{s} = 8\,{\rm TeV}$. Given the limited statistical precision, the data sets are combined to measure the production cross-sections. The LHCb detector and the simulated event samples are outlined in Sect. 2. In Sect. 3 selection criteria are discussed, which exploit the absence of detector activity other than that associated with the $\Upsilon(nS)$ candidate. The signal efficiency and the various sources of background

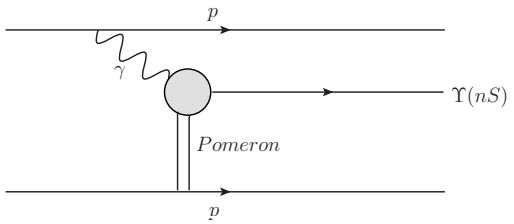

Figure 1: Leading Feynman diagram for photoproduction of $\Upsilon(nS)$ states, where the photon-pomeron interaction is indicated by the shaded grey circle.

are also described. In Sect. 4 two fits are described, which allow the determination of the exclusive signal yield: by fitting the $\Upsilon(nS)$ invariant mass spectrum in order to separate Υ resonances from dimuon continuum background; and by fitting the $\Upsilon(nS)$ candidate $p_{\rm T}^2$ distribution to distinguish exclusively produced Υ resonances from those originating in hard interactions. Systematic uncertainties are summarised in Sect. 5, and the measurements of the cross-sections are discussed in Sect. 6. Finally, for the $\Upsilon(1S)$ the differential cross-section, as a function of $\Upsilon(1S)$ candidate rapidity, is presented.

2 Detector and simulation

The LHCb detector [14, 15] is a single-arm forward spectrometer, designed for the study of particles containing b or c quarks. It is fully instrumented in the pseudorapidity range $2 < \eta < 5$ and has tracking capability in the backward direction, in the range $-3.5 < \eta < -1.5$. The detector includes a high-precision tracking system consisting of a silicon-strip vertex detector (VELO) surrounding the pp interaction region, a large-area silicon-strip detector located upstream of a dipole magnet with a bending power of about 4 Tm, and three stations of silicon-strip detectors and straw drift tubes placed downstream of the magnet. The tracking system provides a measurement of momentum, p, of charged particles with a relative uncertainty that varies from 0.5% at low momentum to 1.0% at 200 GeV/c. Photons, electrons and hadrons are identified by a calorimeter system consisting of scintillating-pad (SPD) and preshower detectors, an electromagnetic calorimeter and a hadronic calorimeter. Muons are identified by a system composed of alternating layers of iron and multiwire proportional chambers.

The trigger consists of a hardware stage, based on information from the calorimeter and muon systems, followed by a software stage, which applies a full event reconstruction. The hardware trigger requires events to contain at least one muon with a $p_{\rm T}$ greater than 200 MeV/c. Low-multiplicity events are selected by requiring that fewer than ten hits should be detected in the scintillating pad detector, positioned just upstream of the electromagnetic calorimeter. In the subsequent software trigger, both of the final-state muons are required to have $p_{\rm T} > 400$ MeV/c.

The exclusive production of $\Upsilon(nS)$ resonances is simulated using the SuperChiC software package [16], which provides the four-momentum of a single, transversely polarised $\Upsilon(nS)$ resonance in each event. The decay of the $\Upsilon(nS)$ candidate is described by EvtGen [17], in which final-state radiation is generated using Photos [18]. The interaction of the generated particles with the detector, and its response, are implemented using the Geant4 toolkit [19] as described in Ref. [20]. Samples, each containing one million events, are prepared for $\Upsilon(nS)$ resonances decaying to $\mu^+\mu^-$. In the same way, nine background samples of a similar size are prepared containing events where an exclusively produced $\chi_{b0,1,2}(1P, 2P, 3P)$ meson decays to the $\Upsilon(nS)\gamma$ final states with $\Upsilon \to \mu^+\mu^-$. Separate samples are prepared for every $\chi_b(mP) \to \Upsilon(nS)\gamma$ $(m, n = 1, 2, 3; n \leq m)$ decay.

3 Candidate selection

Selection criteria are applied offline to events that pass the trigger requirements, to select well-reconstructed $\Upsilon(nS)$ candidates and to ensure the absence of unrelated detector activity. The latter set of requirements favours events containing a single pp interaction per bunch crossing.

The final-state tracks, which must be associated with hits in the muon chambers, are required to lie in the pseudorapidity range $2 < \eta(\mu^{\pm}) < 4.5$ and to be of good quality. In extracting the differential cross-section for the $\Upsilon(1S)$, the following intervals in $\Upsilon(1S)$ rapidity are considered: $2 < y < 3$, $3 < y < 3.5$ and $3.5 < y < 4.5$. Dimuon candidates are selected if the invariant mass falls in the range between $9\,\mathrm{GeV}/c^2$ and $20\,\mathrm{GeV}/c^2$, and the candidate p_{T}^2 is less than $2\,\mathrm{GeV}^2/c^2$. The latter requirement favours photoproduction candidates, which have a characteristically low-p_{T}. Events are rejected if one or more tracks are reconstructed in the backward direction. In the forward region exactly two tracks, corresponding to the muon candidates, are required, and these must be reconstructed both in the VELO and in the downstream tracking detectors.

The selection criteria affect not only the $\Upsilon(nS)$ candidate but also the level of activity in the rest of the event, specifically through the requirements that there should be exactly two forward tracks, no backward tracks and fewer than ten SPD hits. The event is excluded if more than one proton-proton interaction occurs, causing a larger number of additional SPD hits or extra tracks to be reconstructed. The probability for an exclusive Υ event not to feature additional activity from another pp interaction in the same beam crossing is determined as the fraction of events containing no activity, according to these criteria, in a randomly accepted, hence unbiased, sample. After subtracting the contribution of the dimuon candidate, an event may contain fewer than eight SPD hits and no reconstructed tracks in the backward direction or tracks in the forward region. The fraction of randomly triggered events passing these criteria, f_{SI}, is found to be $(23.63 \pm 0.04)\%$ for the 7 TeV data and $(18.48 \pm 0.02)\%$ for the 8 TeV data. The difference arises because of the different beam conditions in the two data-taking periods, leading to a different average number of proton-proton interactions per event.

The reconstruction, trigger and offline selection efficiencies are determined using simulated samples, and the combined efficiency varies between 77% and 84%. For signal candidates that pass the trigger and reconstruction stages, the offline selection criteria are more than 99% efficient.

4 Determining the exclusive yield

Candidates reconstructed in the 7 TeV and 8 TeV data sets are combined in a single sample, and two unbinned, extended, maximum-likelihood fits are carried out. A first fit is performed to the dimuon invariant mass spectrum, between $9\,\mathrm{GeV}/c^2$ and $20\,\mathrm{GeV}/c^2$. The fit contains a non-resonant background component and three resonant components. The three resonant components each receive contributions from exclusive signal, inelastic

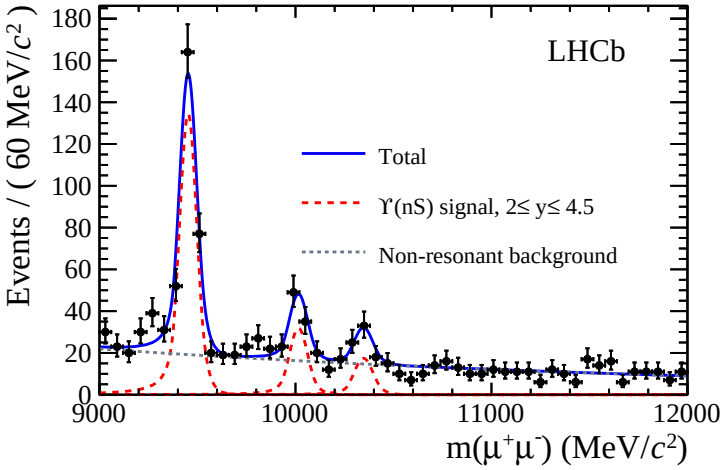

Figure 2: Invariant dimuon mass spectrum for 7 TeV and 8 TeV data in the rapidity range $2 < y(\Upsilon) < 4.5$ (black points). The fit PDF is superimposed (solid blue line). The $\Upsilon(1S, 2S, 3S)$ signal components, used to derive weights, are indicated with a long-dashed (red) line, and the non-resonant background is marked with a short-dashed (grey) line.

Table 1: Results of the invariant mass fits, within each rapidity interval.

Parameter	$2 < y < 4.5$	$2 < y < 3$	$3 < y < 3.5$	$3.5 < y < 4.5$
$\Upsilon(1S, 2S, 3S)$ yield	382 ± 26	146 ± 16	133 ± 16	94 ± 14
$\Upsilon(1S)$ fraction	0.71 ± 0.03	0.74 ± 0.05	0.72 ± 0.06	0.68 ± 0.07
$\Upsilon(2S)$ fraction	0.18 ± 0.03	0.16 ± 0.04	0.15 ± 0.05	0.26 ± 0.06
$\Upsilon(1S)$ mass (MeV/c^2)	9452.5 ± 3.3	9453.2 ± 4.3	9452.4 ± 5.6	9452.0 ± 9.0

background and $\chi_b \to \Upsilon\gamma$ feed-down decays. These contributions are indistinguishable in the invariant mass distribution.

The probability density function (PDF) used to model each $\Upsilon(nS)$ signal peak is a Gaussian function with modified tails (a double-sided crystal ball function [21]). The mass differences for the $\Upsilon(2S)-\Upsilon(1S)$ and $\Upsilon(3S)-\Upsilon(1S)$ resonances are taken from Ref. [22]. The ratios of the $\Upsilon(2S)$ and $\Upsilon(3S)$ resolutions with respect to the $\Upsilon(1S)$ are fixed to the ratio of their masses with respect to the mass of the $\Upsilon(1S)$, following the procedure used in previous Υ measurements using LHCb data [23]. The parameters that govern the shapes of the tails are taken from simulation, as is the resolution of the $\Upsilon(1S)$ resonance, which varies from 35 MeV/c^2 to 57 MeV/c^2 in the different rapidity ranges. The yields of the signal components are all free to vary independently.

A background PDF accounting for the non-resonant background is modelled using an exponential shape where the slope and normalisation are allowed to vary.

The data are fitted in the whole rapidity range and in bins of rapidity. The fit results are given in Table 1 and the fit in the full rapidity range is shown between 9 GeV/c^2 and 12 GeV/c^2 in Fig. 2.

Table 2: Estimated yields of feed-down background from $\chi_b(mP) \to \Upsilon(nS)\gamma$ decays in each $\Upsilon(nS)$ sample, where the uncertainties are statistical only.

Signal window	Υ sample	Estimated contamination yield		
		$\chi_b(1P)$	$\chi_b(2P)$	$\chi_b(3P)$
$2 < y(\Upsilon) < 4.5$	$\Upsilon(1S)$	63 ± 10	14 ± 5	3 ± 2
	$\Upsilon(2S)$	–	43 ± 12	5 ± 3
	$\Upsilon(3S)$	–	–	21 ± 21
$2 < y(\Upsilon) < 3$	$\Upsilon(1S)$	31 ± 8	2 ± 2	0 ± 2
$3 < y(\Upsilon) < 3.5$	$\Upsilon(1S)$	22 ± 6	10 ± 4	0 ± 2
$3.5 < y(\Upsilon) < 4.5$	$\Upsilon(1S)$	8 ± 4	0 ± 2	3 ± 2

Two sources of background contribute to the fitted signal: feed-down from $\chi_b \to \Upsilon\gamma$ decays, and inelastic interactions that involve the undetected products of proton dissociation or additional gluon radiation.

The feed-down background is estimated using a combination of data and simulation, considering $\chi_b(mP) \to \Upsilon(nS)\gamma$ decays. Events are considered in the data set if exactly one photon is found in addition to the Υ candidate. Regions in the $\Upsilon\gamma$ invariant mass spectrum are defined, corresponding to the $\chi_b(1P, 2P, 3P)$ states, and the number of χ_b candidates, N_{χ_b}, for each decay $\chi_b(mP) \to \Upsilon(nS)\gamma$ is counted. An estimate of the total feed-down content of the Υ data sample from each χ_b state is found using the expression:

$$N_{\text{feed-down, } \chi_b(mP)\to\Upsilon(nS)\gamma} = \frac{N_{\chi_b} \times \mathcal{F}}{\epsilon_\gamma \times \epsilon_{\text{mass-range}}}. \quad (1)$$

Here $\mathcal{F}$ is the purity of the $\Upsilon(nS)$ in the corresponding mass window with respect to the non-resonant $\mu^+\mu^-\gamma$ background, determined by fitting the dimuon mass spectrum for events with exactly one reconstructed photon; ϵ_γ is the efficiency for reconstructing the photon produced in each $\chi_b(mP)$ decay, determined using simulated exclusive $\chi_b(mP) \to \Upsilon(nS)\gamma$ decays; and $\epsilon_{\text{mass-range}} = 0.9$ corrects for the fraction of signal Υ candidates which are expected to fall outside the mass window. There are too few $\Upsilon(3S)\gamma$ candidates to estimate the purity precisely so it is assumed to be 100%. Because of limited mass resolution and small sample sizes the χ_b spin states cannot be resolved, so equal contributions from the $\chi_{b1}(mP)$ and $\chi_{b2}(mP)$ states are assumed. The χ_{b0} radiative decay rate is expected to be relatively suppressed and is therefore neglected [22]. The feed-down background yields are given in Table 2.

Since the mass shapes for signal and background do not significantly depend on $p_{\rm T}$ over the $p_{\rm T}$ range considered, the $p_{\rm T}^2$ distribution of the Υ candidates is determined using the *sPlot* technique [24]. A fit is then performed to the $p_{\rm T}^2$ distribution, shown in Fig. 3, using candidates in the full rapidity range $2.0 < y(\Upsilon) < 4.5$, with fit components corresponding to the Υ signal, inelastic background and feed-down background. The fraction of exclusive signal calculated from this fit is assumed to be the same for each rapidity bin.

The $p_{\rm T}^2$ distribution for the exclusive signal is derived from the simulated sample. At HERA, the distribution of the exclusive charmonium signal as a function of the

candidate $p_{\rm T}^2$ was well described by an exponential function, $\exp(-bp_{\rm T}^2)$ [6, 9]. The $p_{\rm T}^2$ distribution provides discrimination among various production sources because it approximates the squared four-momentum transfer, $|t|$, which depends on the production mechanism. Following Ref. [12], Regge phenomenology is used to extrapolate the slope measured by HERA up to LHC energies according to the expression

$$b(W) = b_0 + 4\alpha' \log\left(\frac{W}{W_0}\right), \tag{2}$$

where α' describes the slope of the exchange Regge trajectory and the constant b_0 is specific for interactions at a given photon-proton centre-of-mass energy, W_0 [1]. The SuperChiC generator [16] models the pomeron-photon exchange and performs this extrapolation. Since the only published measurement of b_Υ has very low precision [8], the generator is tuned to reproduce the LHCb measurement of $b_{J/\psi} = 5.7 \pm 0.1$ GeV$^{-2}c^2$ [12] in exclusive J/ψ production. The input values to SuperChiC are $b_0 = 5.6$ GeV$^{-2}c^2$, $\alpha' = 0.2$ GeV$^{-2}c^2$ and $W_0 = 90$ GeV. The fit PDF is obtained from the simulated samples with these inputs, and a kernel estimation is employed to derive a shape to fit to data [25]. It is assumed that the inelastic background component is distributed according to a single exponential function [12]. The slope and yield of this background function are free to vary in the fit.

The total contamination from $\chi_b(mP) \to \Upsilon(nS)\gamma$ decays is constrained to be the sum of the contributions in Table 2 and enters the $p_{\rm T}^2$ fit by means of a Gaussian constraint. Given that no analysis of exclusive χ_b production has been undertaken, and the consequent lack of knowledge of the exclusive purity of the very small sample of reconstructed χ_b candidates, it is assumed that inelastic processes contribute half of this feed-down background and the same inelastic background PDF is employed as that used to model inelastic $\Upsilon(nS)$ production. For the exclusive component, the shape of the dimuon $p_{\rm T}^2$ PDF depends on the $\chi_b(mP)$ meson source, and the PDFs for each source, determined from simulation, are combined according to their relative contributions to the total feed-down yield.

The exclusive purity, $\mathcal{P}$, is defined as the ratio of the exclusive signal yield, $N_{\rm exclusive}$, to the number of candidates remaining in the sample, $N_{\rm exclusive} + N_{\rm inelastic}$, after subtraction of the feed-down yield. The fit to the $p_{\rm T}^2$ distribution in the full rapidity range, shown in Fig. 3, gives

$$\mathcal{P} \equiv \frac{N_{\rm exclusive}}{N_{\rm exclusive} + N_{\rm inelastic}} = (54 \pm 11)\,\%,$$

with the exponential slope of the inelastic background measured to be $-0.21 \pm 0.26\,\text{GeV}^{-2}c^2$. The results of fits to the $p_{\rm T}^2$ distribution in each rapidity interval are consistent with this value. In order to validate the fit procedure, a set of pseudoexperiments is generated using the parameters obtained from the fit to the data, and the same fit is applied to each pseudoexperiment. The uncertainty on the purity is underestimated by 15% in the fit and the statistical uncertainty quoted takes account of this.

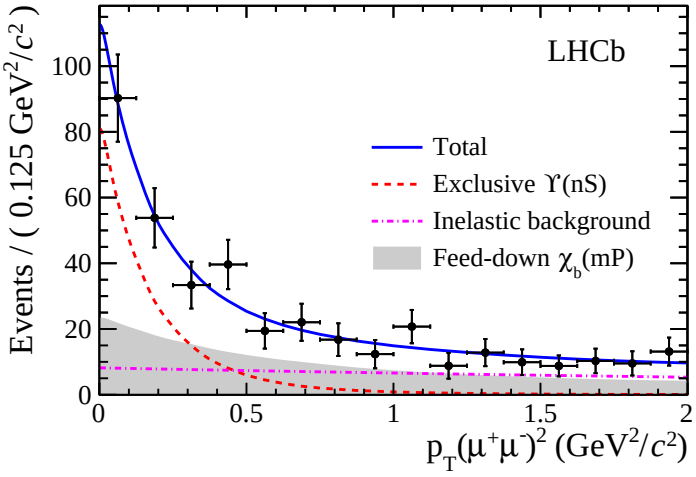

Figure 3: Fit to the $p_{\rm T}^2$ distribution of the Υ candidates in the full rapidity range.

5 Systematic uncertainties

The relative systematic uncertainties for the $\Upsilon(1S, 2S, 3S)$ cross-sections in the various rapidity ranges are summarised in Table 3.

Contributions to the systematic uncertainty arising from the $p_{\rm T}^2$ fit are considered: the uncertainty in the signal $p_{\rm T}^2$ distribution as modelled by the SuperChiC generator and the variation of the exclusive signal PDF expected in the various rapidity bins. The SuperChiC generator is tuned to reproduce measurements of exclusive J/ψ meson production made by LHCb [12]. As no sufficiently precise measurements of the $p_{\rm T}^2$ distribution in exclusive $\Upsilon(nS)$ resonance production exist, an estimate is made following Ref. [1], where it is argued from Regge theory that the slope b_0 of the proton should be reduced by $4\alpha' \log(m_{\Upsilon(nS)}/m_{J/\psi})$. A simulated sample is generated accordingly and used to derive a signal $p_{\rm T}^2$ template. Changing b_0 from 5.6 to 4.7 produces a relative decrease in the exclusive yields of 6%, and this change is taken as the systematic uncertainty. For the differential cross-section measurements, the dependence of the signal $p_{\rm T}^2$ shape on rapidity is studied by replacing the exclusive signal $p_{\rm T}^2$ PDF with those determined in the smaller rapidity ranges, and the largest change in purity is taken as the uncertainty. Combining the systematic uncertainties in quadrature yields a total uncertainty for the exclusive purity, $\mathcal{P}$, between 7.2% and 8.2%. In addition, the possibility for variation in the shape of the continuum dimuon background in $p_{\rm T}^2$ as a function of mass is considered. The determination of the exclusive purity, $\mathcal{P}$, is repeated in the dimuon invariant mass range from 9 to 12 GeV/c^2, and the difference is taken as a conservative estimate of the systematic uncertainty. In Table 3 these sources contribute to the uncertainty denoted 'purity fit'.

The uncertainty arising from the $p_{\rm T}^2$ shape derived from simulation and used to describe the feed-down background is considered separately. The feed-down background PDF is constructed using only contributions from the $\chi_{b1}(mP)$ and $\chi_{b2}(mP)$ background

components, in equal parts, assuming no contribution from $\chi_{b0}(mP)$ decays. Since it is not possible to resolve the spin states in data, we consider a conservative change where the nominal PDF is replaced with that for background originating from the decay of a $\chi_{b0}(mP)$ meson. The fit to data is repeated and the change in exclusive purity is taken as the associated uncertainty. In addition, there is uncertainty associated with the exclusive fraction of the $\chi_b(mP)$ feed-down background, which in turn affects the overall shape of the feed-down background used in the $p_{\rm T}^2$ spectrum. Since the size of the data set is too small to allow a data-driven estimate of the $\chi_b(mP)$ sample exclusive purity, the PDF for this purity is assumed to be uniform between 0% and 100%, and the effect of changing it by ± 1 standard deviation (0.50 ± 0.29) is therefore considered. The resulting change in the exclusive $\Upsilon(nS)$ sample purity is taken as the systematic uncertainty. The estimate of the yield of $\chi_b(mP)$ meson feed-down in data includes the determination of the photon reconstruction efficiency using simulated samples of $\chi_b(mP) \to \Upsilon(nS)\gamma$ decays. Samples of $B^\pm \to J\psi K^{*\pm}(\to K^\pm\pi^0)$ and $B^\pm \to J/\psi K^\pm$ decays are used to validate the agreement between photon reconstruction efficiencies in data and simulation. An uncertainty of 5% is taken as the systematic uncertainty on the photon reconstruction efficiency to account for the small differences seen [26]. The resulting uncertainty is very small for the $\Upsilon(1S)$ but larger for the $\Upsilon(2S, 3S)$ samples where the relative contamination from the $\chi_b(mP)$ background is larger. These three systematic uncertainties on the cross-section are combined in quadrature and are presented as the 'feed-down b.g.' systematic uncertainty in Table 3.

An estimate of the contamination of the $\Upsilon(1S)$ and $\Upsilon(2S)$ samples from the decays $\Upsilon(2S) \to \Upsilon(1S)\pi^0\pi^0$, $\Upsilon(3S) \to \Upsilon(2S)\{\pi^0\pi^0, \gamma\gamma\}$, is made using the observed $\Upsilon(nS)$ candidate yields in data and the relevant $\Upsilon' \to \Upsilon X$ and $\Upsilon^{(\prime)} \to \mu^+\mu^-$ branching fractions [22]. The estimated contaminations are taken as systematic uncertainties for the $\Upsilon(1S)$ and $\Upsilon(2S)$ cross-sections.

Uncertainties in the PDFs used to fit the $\Upsilon(nS)$ candidate invariant mass spectrum are considered. Alternative $\Upsilon(nS)$ signal PDFs are produced, obtained using kernel estimation. The systematic uncertainties on the exclusive purity and each of the yields are assessed using pseudoexperiments generated with the nominal invariant mass PDFs and fitted with a model where the signal PDFs are replaced by those obtained using kernel estimation. The effect of replacing the exponential PDF used to model the non-resonant background in the invariant mass fit with a second-order polynomial function is found in the same way using pseudoexperiments. Combining these two sources of uncertainty in quadrature leads to a relative uncertainty which is less than 4% for all the cross-sections. This uncertainty is labelled 'mass fit' in Table 3.

The LHCb integrated luminosity has been measured with a relative uncertainty of 1.7% at 7 TeV and 1.2% at 8 TeV [27]. The integrated luminosity is multiplied by the estimated, selection-dependent, fraction of events that contain no interactions other than the one that produces the signal candidate, $f_{\rm SI}$. The determination of $f_{\rm SI}$ from data depends upon the subtraction of the Υ signal candidate's SPD hits. The spread in the signal candidate SPD hit multiplicity is estimated from data to be one hit, and the fraction $f_{\rm SI}$ is therefore recomputed with the signal subtraction increased from two to three and the

Table 3: Summary of the relative systematic uncertainties, in %.

	$2<y<3$	$3<y<3.5$	$3.5<y<4.5$	$2<y<4.5$		
	$\Upsilon(1S)$	$\Upsilon(1S)$	$\Upsilon(1S)$	$\Upsilon(1S)$	$\Upsilon(2S)$	$\Upsilon(3S)$
Purity fit	14.2	14.2	14.2	13.7	13.7	13.7
Feed-down b.g.	12.2	12.2	12.3	12.2	14.6	12.5
Υ' feed-down	4.0	4.3	5.4	4.5	11.1	–
Mass fit	2.2	2.8	2.9	2.1	2.8	3.6
Luminosity	2.3	2.3	2.3	2.3	2.3	2.3
$\mathcal{B}(\Upsilon \to \mu^+\mu^-)$	2.0	2.0	2.0	2.0	8.8	9.6
Total	19.5	19.7	20.0	19.3	24.8	21.4

change is taken to be the systematic uncertainty. To account for variations as a function of data-taking time, the variation of the estimated single-interaction fraction is evaluated in each uninterrupted period of data-taking during which conditions are constant, typically an hour long, instead of considering each year as a whole, and the change with respect to the nominal fraction is taken as the systematic uncertainty. Combining the uncertainties in quadrature yields an overall relative uncertainty for each year of 2.3%. The systematic uncertainties on the luminosity for each year are assumed to be 100% correlated.

The branching fractions, $\mathcal{B}$, for $\Upsilon(1S)$, $\Upsilon(2S)$ and $\Upsilon(3S)$ to decay to the dimuon final state are accounted for to determine the $\Upsilon(nS)$ production cross-section. These branching fractions are taken from Ref. [22] and, for the $\Upsilon(1S)$, $\Upsilon(2S)$ and $\Upsilon(3S)$ states, carry relative uncertainties of 2%, 9% and 10%, respectively. These are propagated to an uncertainty on the production cross-section.

6 Cross-section

The cross-section is obtained using

$$\sigma = \frac{N_{\rm exclusive}}{\mathcal{L} \times \epsilon \times \mathcal{B}(\Upsilon(nS) \to \mu^+\mu^-)}. \tag{3}$$

The effective integrated luminosity, $\mathcal{L}$, is $580\,{\rm pb}^{-1}$, taking into account the values of $f_{\rm SI}$ given in Sect. 3 [27].

The quantity ϵ is the efficiency correction, which is obtained in each rapidity bin and for each resonance, and which is averaged for 7 TeV and 8 TeV data according to the luminosity in each year, and $\mathcal{B}(\Upsilon(nS) \to \mu^+\mu^-)$ is the $\Upsilon(nS) \to \mu^+\mu^-$ branching fraction. The measured exclusive production cross-sections in the LHCb acceptance are

$$\begin{aligned}
\sigma(pp \to p\Upsilon(1S)p) &= 9.0 \pm 2.1 \pm 1.7 \text{ pb}, \\
\sigma(pp \to p\Upsilon(2S)p) &= 1.3 \pm 0.8 \pm 0.3 \text{ pb, and} \\
\sigma(pp \to p\Upsilon(3S)p) &< 3.4 \text{ pb at the 95\% confidence level,}
\end{aligned}$$

Table 4: Production cross-section for the $\Upsilon(1S)$ resonance in ranges of $\Upsilon(1S)$ rapidity, where the muons are required to lie in the pseudorapidity range $2 < \eta(\mu^{\pm}) < 4.5$. The first uncertainties are statistical and the second are systematic.

	$2 < y < 3$	$3 < y < 3.5$	$3.5 < y < 4.5$
$\sigma(\Upsilon(1S))$ (pb)	$3.4 \pm 0.9 \pm 0.7$	$2.9 \pm 0.8 \pm 0.6$	$2.6 \pm 0.8 \pm 0.5$

Table 5: Measured $d\sigma(\Upsilon(1S))/dy$, where the data have been corrected for the effect of the LHCb geometrical acceptance. The statistical and systematic uncertainties are combined in quadrature.

	$2 < y < 3$	$3 < y < 3.5$	$3.5 < y < 4.5$
$d\sigma(\Upsilon(1S))/dy$ (pb)	8.8 ± 3.0	7.8 ± 2.7	7.1 ± 2.6

where the first uncertainties are statistical and the second are systematic, and where the limit on $\sigma(\Upsilon(3S))$ includes possible contamination from χ_b feed-down. The limit is calculated using pseudo-experiments and includes the effect of systematic uncertainties, where correlations are assumed to be negligible. The $\Upsilon(1S)$ production cross-section is given in smaller ranges of $\Upsilon(1S)$ rapidity in Table 4.

After correction for the LHCb geometrical acceptance, the cross-sections in Table 4 can be compared to theoretical predictions. The efficiency for an Υ candidate to be produced in the range $2 < y(\Upsilon) < 4.5$, and to decay to muons which lie inside the acceptance, $2 < \eta(\mu^{\pm}) < 4.5$, is 45%. In the smaller ranges of $\Upsilon(1S)$ rapidity considered for the differential cross-section measurement, the efficiency is lowest in the outer ranges, at 39% ($2 < y < 3$) and 36% ($3.5 < y < 4.5$), and highest in the central range, at around 74% ($3 < y < 3.5$). The correction depends on the rapidity distribution in the simulated sample, which has a different shape to those of, for example, the predictions in Fig. 4a. To estimate the systematic uncertainty on the geometrical acceptance correction, the simulated samples are reweighted to obtain a uniform rapidity distribution within each rapidity bin, and the change in the geometrical acceptance is taken as the systematic uncertainty. This corresponds to a relative change in the geometrical acceptance of less than 6%. The differential cross-sections, $d\sigma(\Upsilon(1S))/dy$ are given in Table 5 and are shown in Fig. 4a compared to LO and NLO predictions [1]. The LHCb data are in good agreement with the NLO prediction.

The LHCb results are also compared to theoretical predictions for the underlying photon-proton cross-section, as a function of the centre-of-mass energy of the photon-proton system, W, as shown in Fig. 4b. There are two contributions to the photoproduction of an $\Upsilon(nS)$ resonance, depending on which proton emits the virtual photon. The pp cross-section is given by

$$\frac{d\sigma^{\rm th}(pp \to p\Upsilon(1S)p)}{dy} = S^2(W_+)\left(k_+\frac{dn}{dk_+}\right)\sigma_+^{\rm th}(\gamma p) + S^2(W_-)\left(k_-\frac{dn}{dk_-}\right)\sigma_-^{\rm th}(\gamma p), \quad (4)$$

where the predictions for the photon-proton cross-section are weighted by absorptive corrections $S^2(W_\pm)$ and the photon fluxes $\frac{dn}{dk_\pm}$ for photons of energy $k_\pm \approx (M_{\Upsilon(nS)}/2)\exp(\pm|y|)$.

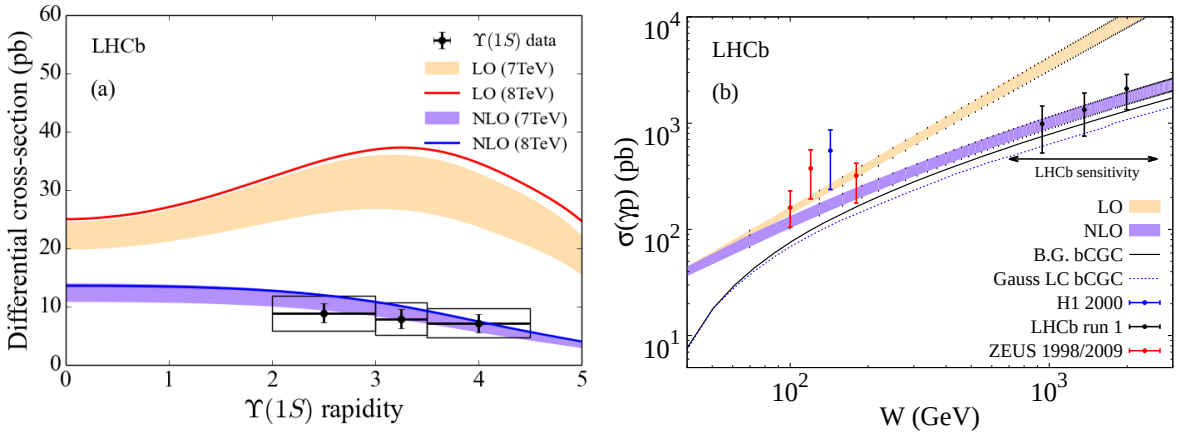

Figure 4: Measurements of exclusive $\Upsilon(1S)$ photoproduction compared to theoretical predictions. In (a), the $\Upsilon(1S)$ cross-section in bins of rapidity is shown, compared to LO and NLO predictions. The LHCb measurements are indicated by black points with error bars for uncorrelated errors, and solid rectangles indicating the total uncertainty. In (b), the photon-proton cross-sections extracted from the LHCb results are indicated by black points, where the statistical and systematic uncertainties are combined in quadrature. The entire W-region in which these LHCb measurements are sensitive is indicated. Measurements made by H1 and ZEUS in the low-W region are indicated by red and blue markers, respectively [4, 5, 7]. Predictions from Ref. [1] are included, resulting from LO and NLO fits to exclusive J/ψ production data. The filled bands indicate the theoretical uncertainties on the 7 TeV prediction and the solid lines indicate the central values of the predictions for 8 TeV. In (b) predictions from Ref. [2] using different models for the $\Upsilon(1S)$ wave function are included, indicated by 'bCGC'.

The absorptive corrections and photon fluxes are computed following Ref. [1].

The three bins of $\Upsilon(1S)$ rapidity chosen in this analysis correspond to ranges of W for the W_+ and W_- solutions. The contribution to the total cross-section from the W_- solutions is expected to be small and is therefore neglected. The dominant W_+ solutions are therefore estimated assuming that they dominate the cross-section, and are shown in Fig. 4b. The magnitude of the theoretical prediction for the W_- solutions is added as a systematic uncertainty. The good agreement with the NLO prediction seen in Fig. 4a is reproduced. The LHCb measurements probe a new kinematic region complementary to that studied at HERA [4, 5, 7], as seen in Fig. 4b, and discriminate between LO and NLO predictions. In Fig. 4b, the LHCb data are also compared to the predictions given in Ref. [2] using models conforming to the colour glass condensate (CGC) formalism [28] that take into account the t-dependence of the differential cross-section. All agree well with the data. The solid (black) and dotted (blue) lines correspond to two different models for the scalar part of the vector-meson wave function.

7 Conclusion

The first measurement of exclusive $\Upsilon(nS)$ production in pp collisions at 7 and 8 TeV is presented, and a differential cross-section is extracted as a function of $\Upsilon(1S)$ candidate rapidity. The data probe a previously unexplored kinematic region in photon-proton centre-of-mass energy. The results are compared to theoretical predictions and a strong preference for those including next-to-leading order calculations is seen. Exclusive production studies at LHCb will be improved during LHC Run II following the installation of scintillators at high $|\eta|$, which will allow for improved trigger efficiency for exclusive production processes and additional suppression of the background from inelastic interactions [29].

Acknowledgements

The authors gratefully acknowledge discussions with Lucian Harland-Lang concerning the implementation and configuration of SuperChiC to model the exclusive production process. We express our gratitude to our colleagues in the CERN accelerator departments for the excellent performance of the LHC. We thank the technical and administrative staff at the LHCb institutes. We acknowledge support from CERN and from the national agencies: CAPES, CNPq, FAPERJ and FINEP (Brazil); NSFC (China); CNRS/IN2P3 (France); BMBF, DFG, HGF and MPG (Germany); INFN (Italy); FOM and NWO (The Netherlands); MNiSW and NCN (Poland); MEN/IFA (Romania); MinES and FANO (Russia); MinECo (Spain); SNSF and SER (Switzerland); NASU (Ukraine); STFC (United Kingdom); NSF (USA). The Tier1 computing centres are supported by IN2P3 (France), KIT and BMBF (Germany), INFN (Italy), NWO and SURF (The Netherlands), PIC (Spain), GridPP (United Kingdom). We are indebted to the communities behind the multiple open source software packages on which we depend. We are also thankful for the computing resources and the access to software R&D tools provided by Yandex LLC (Russia). Individual groups or members have received support from EPLANET, Marie Skłodowska-Curie Actions and ERC (European Union), Conseil général de Haute-Savoie, Labex ENIGMASS and OCEVU, Région Auvergne (France), RFBR (Russia), XuntaGal and GENCAT (Spain), Royal Society and Royal Commission for the Exhibition of 1851 (United Kingdom).

References

[1] S. P. Jones, A. D. Martin, M. G. Ryskin, and T. Teubner, *Probes of the small x gluon via exclusive J/ψ and Υ production at HERA and the LHC*, JHEP **1311** (2013) 085, arXiv:1307.7099.

[2] V. P. Gonçalves, B. D. Moreira, and F. S. Navarra, *Exclusive Υ photoproduction in hadronic collisions at CERN LHC energies*, Phys. Lett. **B742** (2015) 172, arXiv:1408.1344.

[3] H. G. Dosch and E. Ferreira, *Scale dependent pomeron intercept in electromagnetic diffractive processes*, arXiv:1503.06649.

[4] ZEUS collaboration, J. Breitweg *et al.*, *Measurement of elastic Υ photoproduction at HERA*, Phys. Lett. **B437** (1998) 432, arXiv:hep-ex/9807020.

[5] H1 collaboration, C. Adloff *et al.*, *Elastic photoproduction of J/ψ and Υ mesons at HERA*, Phys. Lett. **B483** (2000) 23, arXiv:hep-ex/0003020.

[6] ZEUS collaboration, S. Chekanov *et al.*, *Exclusive photoproduction of J/ψ mesons at HERA*, Eur. Phys. J. **C24** (2002) 345, arXiv:hep-ex/0201043.

[7] ZEUS collaboration, S. Chekanov *et al.*, *Exclusive photoproduction of Υ mesons at HERA*, Phys. Lett. **B680** (2009) 4, arXiv:0903.4205.

[8] ZEUS collaboration, H. Abramowicz *et al.*, *Measurement of the t dependence in exclusive photoproduction of $\Upsilon(1S)$ mesons at HERA*, Phys. Lett. **B708** (2012) 14, arXiv:1111.2133.

[9] H1 collaboration, C. Alexa *et al.*, *Elastic and proton-dissociative photoproduction of J/ψ mesons at HERA*, Eur. Phys. J. **C73** (2013) 2466, arXiv:1304.5162.

[10] CDF collaboration, T. Aaltonen *et al.*, *Observation of exclusive charmonium production and $\gamma + \gamma \to \mu^+\mu^-$ in $p\bar{p}$ collisions at $\sqrt{s} = 1.96$ TeV*, Phys. Rev. Lett. **102** (2009) 242001, arXiv:0902.1271.

[11] ALICE, B. Abelev *et al.*, *Coherent J/ψ photoproduction in ultra-peripheral Pb-Pb collisions at $\sqrt{s_{NN}} = 2.76$ TeV*, Phys. Lett. **B718** (2013) 1273, arXiv:1209.3715.

[12] LHCb collaboration, R. Aaij *et al.*, *Updated measurements of exclusive J/ψ and $\psi(2S)$ production cross-sections in pp collisions at $\sqrt{s} = 7$ TeV*, J. Phys. **G41** (2014) 055002, arXiv:1401.3288.

[13] ALICE, B. B. Abelev *et al.*, *Exclusive J/ψ photoproduction off protons in ultra-peripheral p-Pb collisions at $\sqrt{s_{\rm NN}} = 5.02$ TeV*, Phys. Rev. Lett. **113** (2014), no. 23 232504, arXiv:1406.7819.

[14] LHCb collaboration, A. A. Alves Jr. *et al.*, *The LHCb detector at the LHC*, JINST **3** (2008) S08005.

[15] LHCb collaboration, R. Aaij *et al.*, *LHCb detector performance*, Int. J. Mod. Phys. **A30** (2015) 1530022, arXiv:1412.6352.

[16] L. A. Harland-Lang, V. A. Khoze, M. G. Ryskin, and W. J. Stirling, *Standard candle central exclusive processes at the Tevatron and LHC*, Eur. Phys. J. **C69** (2010) 179, arXiv:1005.0695.

[17] D. J. Lange, *The EvtGen particle decay simulation package*, Nucl. Instrum. Meth. **A462** (2001) 152.

[18] P. Golonka and Z. Was, *PHOTOS Monte Carlo: A precision tool for QED corrections in Z and W decays*, Eur. Phys. J. **C45** (2006) 97, arXiv:hep-ph/0506026.

[19] Geant4 collaboration, J. Allison *et al.*, *Geant4 developments and applications*, IEEE Trans. Nucl. Sci. **53** (2006) 270; Geant4 collaboration, S. Agostinelli *et al.*, *Geant4: A simulation toolkit*, Nucl. Instrum. Meth. **A506** (2003) 250.

[20] M. Clemencic *et al.*, *The LHCb simulation application, Gauss: Design, evolution and experience*, J. Phys. Conf. Ser. **331** (2011) 032023.

[21] T. Skwarnicki, *A study of the radiative cascade transitions between the Υ' and Υ resonances*, PhD thesis, Institute of Nuclear Physics, Krakow, 1986, DESY-F31-86-02.

[22] Particle Data Group, K. A. Olive *et al.*, *Review of particle physics*, Chin. Phys. **C38** (2014) 090001.

[23] LHCb collaboration, R. Aaij *et al.*, *Measurement of Υ production in pp collisions at $\sqrt{s} = 7$ TeV*, Eur. Phys. J. **C72** (2012) 2025, arXiv:1202.6579.

[24] M. Pivk and F. R. Le Diberder, *sPlot: A statistical tool to unfold data distributions*, Nucl. Instrum. Meth. **A555** (2005) 356, arXiv:physics/0402083.

[25] K. S. Cranmer, *Kernel estimation in high-energy physics*, Comput. Phys. Commun. **136** (2001) 198, arXiv:hep-ex/0011057.

[26] E. Govorkova, *Study of photon reconstruction efficiency using $B^+ \to J/\psi K^{(*)+}$ decays in the LHCb experiment*, arXiv:1505.02960.

[27] LHCb collaboration, R. Aaij *et al.*, *Precision luminosity measurements at LHCb*, JINST **9** (2014) P12005, arXiv:1410.0149.

[28] J. Jalilian-Marian, A. Kovner, L. D. McLerran, and H. Weigert, *The intrinsic glue distribution at very small x*, Phys. Rev. **D55** (1997) 5414, arXiv:hep-ph/9606337.

[29] FSC Team (CMS), HERSCHEL Team (LHCb), M. Albrow, P. Collins, and A. Penzo, *Forward shower counters for diffractive physics at the LHC*, Int. J. Mod. Phys. **A29** (2014) 1446018.

LHCb collaboration

R. Aaij[38], B. Adeva[37], M. Adinolfi[46], A. Affolder[52], Z. Ajaltouni[5], S. Akar[6], J. Albrecht[9], F. Alessio[38], M. Alexander[51], S. Ali[41], G. Alkhazov[30], P. Alvarez Cartelle[53], A.A. Alves Jr[57], S. Amato[2], S. Amerio[22], Y. Amhis[7], L. An[3], L. Anderlini[17,g], J. Anderson[40], M. Andreotti[16,f], J.E. Andrews[58], R.B. Appleby[54], O. Aquines Gutierrez[10], F. Archilli[38], P. d'Argent[11], A. Artamonov[35], M. Artuso[59], E. Aslanides[6], G. Auriemma[25,n], M. Baalouch[5], S. Bachmann[11], J.J. Back[48], A. Badalov[36], C. Baesso[60], W. Baldini[16,38], R.J. Barlow[54], C. Barschel[38], S. Barsuk[7], W. Barter[38], V. Batozskaya[28], V. Battista[39], A. Bay[39], L. Beaucourt[4], J. Beddow[51], F. Bedeschi[23], I. Bediaga[1], L.J. Bel[41], I. Belyaev[31], E. Ben-Haim[8], G. Bencivenni[18], S. Benson[38], J. Benton[46], A. Berezhnoy[32], R. Bernet[40], A. Bertolin[22], M.-O. Bettler[38], M. van Beuzekom[41], A. Bien[11], S. Bifani[45], T. Bird[54], A. Birnkraut[9], A. Bizzeti[17,i], T. Blake[48], F. Blanc[39], J. Blouw[10], S. Blusk[59], V. Bocci[25], A. Bondar[34], N. Bondar[30,38], W. Bonivento[15], S. Borghi[54], M. Borsato[7], T.J.V. Bowcock[52], E. Bowen[40], C. Bozzi[16], S. Braun[11], D. Brett[54], M. Britsch[10], T. Britton[59], J. Brodzicka[54], N.H. Brook[46], A. Bursche[40], J. Buytaert[38], S. Cadeddu[15], R. Calabrese[16,f], M. Calvi[20,k], M. Calvo Gomez[36,p], P. Campana[18], D. Campora Perez[38], L. Capriotti[54], A. Carbone[14,d], G. Carboni[24,l], R. Cardinale[19,j], A. Cardini[15], P. Carniti[20], L. Carson[50], K. Carvalho Akiba[2,38], R. Casanova Mohr[36], G. Casse[52], L. Cassina[20,k], L. Castillo Garcia[38], M. Cattaneo[38], Ch. Cauet[9], G. Cavallero[19], R. Cenci[23,t], M. Charles[8], Ph. Charpentier[38], M. Chefdeville[4], S. Chen[54], S.-F. Cheung[55], N. Chiapolini[40], M. Chrzaszcz[40,26], X. Cid Vidal[38], G. Ciezarek[41], P.E.L. Clarke[50], M. Clemencic[38], H.V. Cliff[47], J. Closier[38], V. Coco[38], J. Cogan[6], E. Cogneras[5], V. Cogoni[15,e], L. Cojocariu[29], G. Collazuol[22], P. Collins[38], A. Comerma-Montells[11], A. Contu[15,38], A. Cook[46], M. Coombes[46], S. Coquereau[8], G. Corti[38], M. Corvo[16,f], B. Couturier[38], G.A. Cowan[50], D.C. Craik[48], A. Crocombe[48], M. Cruz Torres[60], S. Cunliffe[53], R. Currie[53], C. D'Ambrosio[38], J. Dalseno[46], P.N.Y. David[41], A. Davis[57], K. De Bruyn[41], S. De Capua[54], M. De Cian[11], J.M. De Miranda[1], L. De Paula[2], W. De Silva[57], P. De Simone[18], C.-T. Dean[51], D. Decamp[4], M. Deckenhoff[9], L. Del Buono[8], N. Déléage[4], D. Derkach[55], O. Deschamps[5], F. Dettori[38], B. Dey[40], A. Di Canto[38], F. Di Ruscio[24], H. Dijkstra[38], S. Donleavy[52], F. Dordei[11], M. Dorigo[39], A. Dosil Suárez[37], D. Dossett[48], A. Dovbnya[43], K. Dreimanis[52], G. Dujany[54], F. Dupertuis[39], P. Durante[38], R. Dzhelyadin[35], A. Dziurda[26], A. Dzyuba[30], S. Easo[49,38], U. Egede[53], V. Egorychev[31], S. Eidelman[34], S. Eisenhardt[50], U. Eitschberger[9], R. Ekelhof[9], L. Eklund[51], I. El Rifai[5], Ch. Elsasser[40], S. Ely[59], S. Esen[11], H.M. Evans[47], T. Evans[55], A. Falabella[14], C. Färber[11], C. Farinelli[41], N. Farley[45], S. Farry[52], R. Fay[52], D. Ferguson[50], V. Fernandez Albor[37], F. Ferrari[14], F. Ferreira Rodrigues[1], M. Ferro-Luzzi[38], S. Filippov[33], M. Fiore[16,38,f], M. Fiorini[16,f], M. Firlej[27], C. Fitzpatrick[39], T. Fiutowski[27], P. Fol[53], M. Fontana[10], F. Fontanelli[19,j], R. Forty[38], O. Francisco[2], M. Frank[38], C. Frei[38], M. Frosini[17], J. Fu[21], E. Furfaro[24,l], A. Gallas Torreira[37], D. Galli[14,d], S. Gallorini[22,38], S. Gambetta[19,j], M. Gandelman[2], P. Gandini[55], Y. Gao[3], J. García Pardiñas[37], J. Garofoli[59], J. Garra Tico[47], L. Garrido[36], D. Gascon[36], C. Gaspar[38], U. Gastaldi[16], R. Gauld[55], L. Gavardi[9], G. Gazzoni[5], A. Geraci[21,v], D. Gerick[11], E. Gersabeck[11], M. Gersabeck[54], T. Gershon[48], Ph. Ghez[4], A. Gianelle[22], S. Gianì[39], V. Gibson[47], L. Giubega[29], V.V. Gligorov[38], C. Göbel[60], D. Golubkov[31], A. Golutvin[53,31,38], A. Gomes[1,a], C. Gotti[20,k], M. Grabalosa Gándara[5], R. Graciani Diaz[36], L.A. Granado Cardoso[38], E. Graugés[36], E. Graverini[40], G. Graziani[17], A. Grecu[29], E. Greening[55], S. Gregson[47], P. Griffith[45], L. Grillo[11], O. Grünberg[63], B. Gui[59], E. Gushchin[33], Yu. Guz[35,38], T. Gys[38], C. Hadjivasiliou[59], G. Haefeli[39], C. Haen[38],

S.C. Haines[47], S. Hall[53], B. Hamilton[58], T. Hampson[46], X. Han[11], S. Hansmann-Menzemer[11], N. Harnew[55], S.T. Harnew[46], J. Harrison[54], J. He[38], T. Head[39], V. Heijne[41], K. Hennessy[52], P. Henrard[5], L. Henry[8], J.A. Hernando Morata[37], E. van Herwijnen[38], M. Heß[63], A. Hicheur[2], D. Hill[55], M. Hoballah[5], C. Hombach[54], W. Hulsbergen[41], T. Humair[53], N. Hussain[55], D. Hutchcroft[52], D. Hynds[51], M. Idzik[27], P. Ilten[56], R. Jacobsson[38], A. Jaeger[11], J. Jalocha[55], E. Jans[41], A. Jawahery[58], F. Jing[3], M. John[55], D. Johnson[38], C.R. Jones[47], C. Joram[38], B. Jost[38], N. Jurik[59], S. Kandybei[43], W. Kanso[6], M. Karacson[38], T.M. Karbach[38,†], S. Karodia[51], M. Kelsey[59], I.R. Kenyon[45], M. Kenzie[38], T. Ketel[42], B. Khanji[20,38,k], C. Khurewathanakul[39], S. Klaver[54], K. Klimaszewski[28], O. Kochebina[7], M. Kolpin[11], I. Komarov[39], R.F. Koopman[42], P. Koppenburg[41,38], M. Korolev[32], L. Kravchuk[33], K. Kreplin[11], M. Kreps[48], G. Krocker[11], P. Krokovny[34], F. Kruse[9], W. Kucewicz[26,o], M. Kucharczyk[26], V. Kudryavtsev[34], K. Kurek[28], T. Kvaratskheliya[31], V.N. La Thi[39], D. Lacarrere[38], G. Lafferty[54], A. Lai[15], D. Lambert[50], R.W. Lambert[42], G. Lanfranchi[18], C. Langenbruch[48], B. Langhans[38], T. Latham[48], C. Lazzeroni[45], R. Le Gac[6], J. van Leerdam[41], J.-P. Lees[4], R. Lefèvre[5], A. Leflat[32], J. Lefrançois[7], O. Leroy[6], T. Lesiak[26], B. Leverington[11], Y. Li[7], T. Likhomanenko[65,64], M. Liles[52], R. Lindner[38], C. Linn[38], F. Lionetto[40], B. Liu[15], S. Lohn[38], I. Longstaff[51], J.H. Lopes[2], D. Lucchesi[22,r], M. Lucio Martinez[37], H. Luo[50], A. Lupato[22], E. Luppi[16,f], O. Lupton[55], F. Machefert[7], F. Maciuc[29], O. Maev[30], S. Malde[55], A. Malinin[64], G. Manca[15,e], G. Mancinelli[6], P. Manning[59], A. Mapelli[38], J. Maratas[5], J.F. Marchand[4], U. Marconi[14], C. Marin Benito[36], P. Marino[23,38,t], R. Märki[39], J. Marks[11], G. Martellotti[25], M. Martinelli[39], D. Martinez Santos[42], F. Martinez Vidal[66], D. Martins Tostes[2], A. Massafferri[1], R. Matev[38], A. Mathad[48], Z. Mathe[38], C. Matteuzzi[20], K. Matthieu[11], A. Mauri[40], B. Maurin[39], A. Mazurov[45], M. McCann[53], J. McCarthy[45], A. McNab[54], R. McNulty[12], B. Meadows[57], F. Meier[9], M. Meissner[11], M. Merk[41], D.A. Milanes[62], M.-N. Minard[4], D.S. Mitzel[11], J. Molina Rodriguez[60], S. Monteil[5], M. Morandin[22], P. Morawski[27], A. Mordà[6], M.J. Morello[23,t], J. Moron[27], A.B. Morris[50], R. Mountain[59], F. Muheim[50], J. Müller[9], K. Müller[40], V. Müller[9], M. Mussini[14], B. Muster[39], P. Naik[46], T. Nakada[39], R. Nandakumar[49], I. Nasteva[2], M. Needham[50], N. Neri[21], S. Neubert[11], N. Neufeld[38], M. Neuner[11], A.D. Nguyen[39], T.D. Nguyen[39], C. Nguyen-Mau[39,q], V. Niess[5], R. Niet[9], N. Nikitin[32], T. Nikodem[11], D. Ninci[23], A. Novoselov[35], D.P. O'Hanlon[48], A. Oblakowska-Mucha[27], V. Obraztsov[35], S. Ogilvy[51], O. Okhrimenko[44], R. Oldeman[15,e], C.J.G. Onderwater[67], B. Osorio Rodrigues[1], J.M. Otalora Goicochea[2], A. Otto[38], P. Owen[53], A. Oyanguren[66], A. Palano[13,c], F. Palombo[21,u], M. Palutan[18], J. Panman[38], A. Papanestis[49], M. Pappagallo[51], L.L. Pappalardo[16,f], C. Parkes[54], G. Passaleva[17], G.D. Patel[52], M. Patel[53], C. Patrignani[19,j], A. Pearce[54,49], A. Pellegrino[41], G. Penso[25,m], M. Pepe Altarelli[38], S. Perazzini[14,d], P. Perret[5], L. Pescatore[45], K. Petridis[46], A. Petrolini[19,j], M. Petruzzo[21], E. Picatoste Olloqui[36], B. Pietrzyk[4], T. Pilař[48], D. Pinci[25], A. Pistone[19], S. Playfer[50], M. Plo Casasus[37], T. Poikela[38], F. Polci[8], A. Poluektov[48,34], I. Polyakov[31], E. Polycarpo[2], A. Popov[35], D. Popov[10], B. Popovici[29], C. Potterat[2], E. Price[46], J.D. Price[52], J. Prisciandaro[39], A. Pritchard[52], C. Prouve[46], V. Pugatch[44], A. Puig Navarro[39], G. Punzi[23,s], W. Qian[4], R. Quagliani[7,46], B. Rachwal[26], J.H. Rademacker[46], B. Rakotomiaramanana[39], M. Rama[23], M.S. Rangel[2], I. Raniuk[43], N. Rauschmayr[38], G. Raven[42], F. Redi[53], S. Reichert[54], M.M. Reid[48], A.C. dos Reis[1], S. Ricciardi[49], S. Richards[46], M. Rihl[38], K. Rinnert[52], V. Rives Molina[36], P. Robbe[7,38], A.B. Rodrigues[1], E. Rodrigues[54], J.A. Rodriguez Lopez[62], P. Rodriguez Perez[54], S. Roiser[38], V. Romanovsky[35], A. Romero Vidal[37], M. Rotondo[22], J. Rouvinet[39], T. Ruf[38], H. Ruiz[36], P. Ruiz Valls[66], J.J. Saborido Silva[37], N. Sagidova[30], P. Sail[51], B. Saitta[15,e], V. Salustino Guimaraes[2],

C. Sanchez Mayordomo[66], B. Sanmartin Sedes[37], R. Santacesaria[25], C. Santamarina Rios[37], E. Santovetti[24,l], A. Sarti[18,m], C. Satriano[25,n], A. Satta[24], D.M. Saunders[46], D. Savrina[31,32], M. Schiller[38], H. Schindler[38], M. Schlupp[9], M. Schmelling[10], T. Schmelzer[9], B. Schmidt[38], O. Schneider[39], A. Schopper[38], M.-H. Schune[7], R. Schwemmer[38], B. Sciascia[18], A. Sciubba[25,m], A. Semennikov[31], I. Sepp[53], N. Serra[40], J. Serrano[6], L. Sestini[22], P. Seyfert[11], M. Shapkin[35], I. Shapoval[16,43,f], Y. Shcheglov[30], T. Shears[52], L. Shekhtman[34], V. Shevchenko[64], A. Shires[9], R. Silva Coutinho[48], G. Simi[22], M. Sirendi[47], N. Skidmore[46], I. Skillicorn[51], T. Skwarnicki[59], E. Smith[55,49], E. Smith[53], J. Smith[47], M. Smith[54], H. Snoek[41], M.D. Sokoloff[57,38], F.J.P. Soler[51], F. Soomro[39], D. Souza[46], B. Souza De Paula[2], B. Spaan[9], P. Spradlin[51], S. Sridharan[38], F. Stagni[38], M. Stahl[11], S. Stahl[38], O. Steinkamp[40], O. Stenyakin[35], F. Sterpka[59], S. Stevenson[55], S. Stoica[29], S. Stone[59], B. Storaci[40], S. Stracka[23,t], M. Straticiuc[29], U. Straumann[40], R. Stroili[22], L. Sun[57], W. Sutcliffe[53], K. Swientek[27], S. Swientek[9], V. Syropoulos[42], M. Szczekowski[28], P. Szczypka[39,38], T. Szumlak[27], S. T'Jampens[4], T. Tekampe[9], M. Teklishyn[7], G. Tellarini[16,f], F. Teubert[38], C. Thomas[55], E. Thomas[38], J. van Tilburg[41], V. Tisserand[4], M. Tobin[39], J. Todd[57], S. Tolk[42], L. Tomassetti[16,f], D. Tonelli[38], S. Topp-Joergensen[55], N. Torr[55], E. Tournefier[4], S. Tourneur[39], K. Trabelsi[39], M.T. Tran[39], M. Tresch[40], A. Trisovic[38], A. Tsaregorodtsev[6], P. Tsopelas[41], N. Tuning[41,38], A. Ukleja[28], A. Ustyuzhanin[65,64], U. Uwer[11], C. Vacca[15,e], V. Vagnoni[14], G. Valenti[14], A. Vallier[7], R. Vazquez Gomez[18], P. Vazquez Regueiro[37], C. Vázquez Sierra[37], S. Vecchi[16], J.J. Velthuis[46], M. Veltri[17,h], G. Veneziano[39], M. Vesterinen[11], B. Viaud[7], D. Vieira[2], M. Vieites Diaz[37], X. Vilasis-Cardona[36,p], A. Vollhardt[40], D. Volyanskyy[10], D. Voong[46], A. Vorobyev[30], V. Vorobyev[34], C. Voß[63], J.A. de Vries[41], R. Waldi[63], C. Wallace[48], R. Wallace[12], J. Walsh[23], S. Wandernoth[11], J. Wang[59], D.R. Ward[47], N.K. Watson[45], D. Websdale[53], A. Weiden[40], M. Whitehead[48], D. Wiedner[11], G. Wilkinson[55,38], M. Wilkinson[59], M. Williams[38], M.P. Williams[45], M. Williams[56], F.F. Wilson[49], J. Wimberley[58], J. Wishahi[9], W. Wislicki[28], M. Witek[26], G. Wormser[7], S.A. Wotton[47], S. Wright[47], K. Wyllie[38], Y. Xie[61], Z. Xu[39], Z. Yang[3], X. Yuan[34], O. Yushchenko[35], M. Zangoli[14], M. Zavertyaev[10,b], L. Zhang[3], Y. Zhang[3], A. Zhelezov[11], A. Zhokhov[31], L. Zhong[3].

[1] *Centro Brasileiro de Pesquisas Físicas (CBPF), Rio de Janeiro, Brazil*
[2] *Universidade Federal do Rio de Janeiro (UFRJ), Rio de Janeiro, Brazil*
[3] *Center for High Energy Physics, Tsinghua University, Beijing, China*
[4] *LAPP, Université Savoie Mont-Blanc, CNRS/IN2P3, Annecy-Le-Vieux, France*
[5] *Clermont Université, Université Blaise Pascal, CNRS/IN2P3, LPC, Clermont-Ferrand, France*
[6] *CPPM, Aix-Marseille Université, CNRS/IN2P3, Marseille, France*
[7] *LAL, Université Paris-Sud, CNRS/IN2P3, Orsay, France*
[8] *LPNHE, Université Pierre et Marie Curie, Université Paris Diderot, CNRS/IN2P3, Paris, France*
[9] *Fakultät Physik, Technische Universität Dortmund, Dortmund, Germany*
[10] *Max-Planck-Institut für Kernphysik (MPIK), Heidelberg, Germany*
[11] *Physikalisches Institut, Ruprecht-Karls-Universität Heidelberg, Heidelberg, Germany*
[12] *School of Physics, University College Dublin, Dublin, Ireland*
[13] *Sezione INFN di Bari, Bari, Italy*
[14] *Sezione INFN di Bologna, Bologna, Italy*
[15] *Sezione INFN di Cagliari, Cagliari, Italy*
[16] *Sezione INFN di Ferrara, Ferrara, Italy*
[17] *Sezione INFN di Firenze, Firenze, Italy*
[18] *Laboratori Nazionali dell'INFN di Frascati, Frascati, Italy*
[19] *Sezione INFN di Genova, Genova, Italy*

[20] *Sezione INFN di Milano Bicocca, Milano, Italy*
[21] *Sezione INFN di Milano, Milano, Italy*
[22] *Sezione INFN di Padova, Padova, Italy*
[23] *Sezione INFN di Pisa, Pisa, Italy*
[24] *Sezione INFN di Roma Tor Vergata, Roma, Italy*
[25] *Sezione INFN di Roma La Sapienza, Roma, Italy*
[26] *Henryk Niewodniczanski Institute of Nuclear Physics Polish Academy of Sciences, Kraków, Poland*
[27] *AGH - University of Science and Technology, Faculty of Physics and Applied Computer Science, Kraków, Poland*
[28] *National Center for Nuclear Research (NCBJ), Warsaw, Poland*
[29] *Horia Hulubei National Institute of Physics and Nuclear Engineering, Bucharest-Magurele, Romania*
[30] *Petersburg Nuclear Physics Institute (PNPI), Gatchina, Russia*
[31] *Institute of Theoretical and Experimental Physics (ITEP), Moscow, Russia*
[32] *Institute of Nuclear Physics, Moscow State University (SINP MSU), Moscow, Russia*
[33] *Institute for Nuclear Research of the Russian Academy of Sciences (INR RAN), Moscow, Russia*
[34] *Budker Institute of Nuclear Physics (SB RAS) and Novosibirsk State University, Novosibirsk, Russia*
[35] *Institute for High Energy Physics (IHEP), Protvino, Russia*
[36] *Universitat de Barcelona, Barcelona, Spain*
[37] *Universidad de Santiago de Compostela, Santiago de Compostela, Spain*
[38] *European Organization for Nuclear Research (CERN), Geneva, Switzerland*
[39] *Ecole Polytechnique Fédérale de Lausanne (EPFL), Lausanne, Switzerland*
[40] *Physik-Institut, Universität Zürich, Zürich, Switzerland*
[41] *Nikhef National Institute for Subatomic Physics, Amsterdam, The Netherlands*
[42] *Nikhef National Institute for Subatomic Physics and VU University Amsterdam, Amsterdam, The Netherlands*
[43] *NSC Kharkiv Institute of Physics and Technology (NSC KIPT), Kharkiv, Ukraine*
[44] *Institute for Nuclear Research of the National Academy of Sciences (KINR), Kyiv, Ukraine*
[45] *University of Birmingham, Birmingham, United Kingdom*
[46] *H.H. Wills Physics Laboratory, University of Bristol, Bristol, United Kingdom*
[47] *Cavendish Laboratory, University of Cambridge, Cambridge, United Kingdom*
[48] *Department of Physics, University of Warwick, Coventry, United Kingdom*
[49] *STFC Rutherford Appleton Laboratory, Didcot, United Kingdom*
[50] *School of Physics and Astronomy, University of Edinburgh, Edinburgh, United Kingdom*
[51] *School of Physics and Astronomy, University of Glasgow, Glasgow, United Kingdom*
[52] *Oliver Lodge Laboratory, University of Liverpool, Liverpool, United Kingdom*
[53] *Imperial College London, London, United Kingdom*
[54] *School of Physics and Astronomy, University of Manchester, Manchester, United Kingdom*
[55] *Department of Physics, University of Oxford, Oxford, United Kingdom*
[56] *Massachusetts Institute of Technology, Cambridge, MA, United States*
[57] *University of Cincinnati, Cincinnati, OH, United States*
[58] *University of Maryland, College Park, MD, United States*
[59] *Syracuse University, Syracuse, NY, United States*
[60] *Pontifícia Universidade Católica do Rio de Janeiro (PUC-Rio), Rio de Janeiro, Brazil, associated to* [2]
[61] *Institute of Particle Physics, Central China Normal University, Wuhan, Hubei, China, associated to* [3]
[62] *Departamento de Fisica , Universidad Nacional de Colombia, Bogota, Colombia, associated to* [8]
[63] *Institut für Physik, Universität Rostock, Rostock, Germany, associated to* [11]
[64] *National Research Centre Kurchatov Institute, Moscow, Russia, associated to* [31]
[65] *Yandex School of Data Analysis, Moscow, Russia, associated to* [31]
[66] *Instituto de Fisica Corpuscular (IFIC), Universitat de Valencia-CSIC, Valencia, Spain, associated to* [36]
[67] *Van Swinderen Institute, University of Groningen, Groningen, The Netherlands, associated to* [41]

[a] *Universidade Federal do Triângulo Mineiro (UFTM), Uberaba-MG, Brazil*

[b] *P.N. Lebedev Physical Institute, Russian Academy of Science (LPI RAS), Moscow, Russia*
[c] *Università di Bari, Bari, Italy*
[d] *Università di Bologna, Bologna, Italy*
[e] *Università di Cagliari, Cagliari, Italy*
[f] *Università di Ferrara, Ferrara, Italy*
[g] *Università di Firenze, Firenze, Italy*
[h] *Università di Urbino, Urbino, Italy*
[i] *Università di Modena e Reggio Emilia, Modena, Italy*
[j] *Università di Genova, Genova, Italy*
[k] *Università di Milano Bicocca, Milano, Italy*
[l] *Università di Roma Tor Vergata, Roma, Italy*
[m] *Università di Roma La Sapienza, Roma, Italy*
[n] *Università della Basilicata, Potenza, Italy*
[o] *AGH - University of Science and Technology, Faculty of Computer Science, Electronics and Telecommunications, Kraków, Poland*
[p] *LIFAELS, La Salle, Universitat Ramon Llull, Barcelona, Spain*
[q] *Hanoi University of Science, Hanoi, Viet Nam*
[r] *Università di Padova, Padova, Italy*
[s] *Università di Pisa, Pisa, Italy*
[t] *Scuola Normale Superiore, Pisa, Italy*
[u] *Università degli Studi di Milano, Milano, Italy*
[v] *Politecnico di Milano, Milano, Italy*

[†] *Deceased*